FINAL REPORT FOR SUBCONTRACT NO. 53250.420 7001

Project Title:	Task Assignment "NSO RF Physics Heating Studies" (DOE Task No. 47)
Principal Investigator:	James R. Myra
Date of Report:	September 30, 1999
Recipient Organization:	Lodestar Research Corporation 2400 Central Avenue #P-5 Boulder, CO 80301
DOE Contract:	Raytheon / Lodestar Subcontract No. 53250.420 7001

NSO RF Physics Heating Studies

J. R. Myra, D. A. D'Ippolito and R. E. Aamodt

Lodestar Research Corporation
Boulder, Colorado

M. D. Carter and E. F. Jaeger

Oak Ridge National Laboratory
Oak Ridge, Tennessee

Executive Summary

This report summarizes studies of Ion Cyclotron Resonance Frequency (ICRF) heating motivated by planning for the Next Step Option (NSO) experiment. Important issues impacting ICRF heating in the proposed IGNITOR[1] and FIRE[2] experiments were studied and are discussed here in separate reports.

Many studies of ICRF resonant ion and minority ion heating scenarios have been carried out for the steady-state phase of IGNITOR, e.g. see the recent work by Riccitelli et al.[3] A remaining critical issue is to determine the feasibility of heating the plasma during the ramp-up of the magnetic field B, plasma current I_p and density n. ICRF heating during the ramp phase would potentially allow an H-mode transition at lower values of these parameters, and hence at lower heating power. Resonant ion heating scenarios are

difficult during the ramp phase because of the problems associated with time-dependent resonant heating surfaces. For this reason, we have investigated a high-frequency electron heating scenario proposed by Majeski.[4] A detailed analysis of the ICRF heating efficiency is presented in the context of a generalized POPCON analysis. The rf absorption was computed using the FREMIR ray tracing code[5] developed by Jacquinot. The conclusion of this study is that the 400 MHz electron heating is feasible, despite low single pass absorption at the beginning of the ramp, and can lead to H-modes at lower auxiliary power.

In contrast with the situation for IGNITOR, no detailed ICRF heating scenarios have been carried out previously. As the FIRE design permits longer pulses than IGNITOR, heating during the steady-state phase is the main interest. We have carried out a survey of two ion heating scenarios, ^{3}He minority and second harmonic T heating at 100 MHz and H minority and second harmonic D heating at 150 MHz, using the FREMIR[5] and ORION1D[6] codes. The dependence on minority concentration and the relative absorption by the various ion species is analyzed for an antenna design proposed by Swain and Carter.[7] It is shown that both frequencies lead to good single pass absorption at small minority fraction.

A second issue for ICRF heating on high edge density machines like IGNITOR and FIRE is the general area of ICRF-edge plasma interactions. One of the most important aspects of ICRF-edge plasma physics is the generation of radio-frequency (rf) sheaths on the antenna structure. Particles accelerated in the sheaths can carry a significant fraction of the coupled ICRF power into the antenna structure itself, leading to reduced heating efficiency and heat damage to the antenna and surrounding limiters. For a given antenna, magnetic field geometry, and rf power, the sheath heating imposes a limit on the density in the vicinity of the antenna. These issues have been studied and quantified for both IGNITOR and FIRE using the RANT3D antenna code[8] and the Lodestar ICRF-edge physics analysis models.[9-11] The conclusion of this study is that in both cases a reasonable heating efficiency and sufficiently small antenna heat load can be obtained if the antenna structure is sufficiently recessed from the main scrape-off-layer (SOL) plasma.

Technical Studies

The following papers are attached to this final report in fulfillment of the subcontract with Raytheon:

A. RF Heating Studies for IGNITOR

B. RF Heating Studies for FIRE

References

1. B. Coppi, M. Nassi and L. E. Sugiyama, Physica Scripta **45**, 112 (1992).
2. "Fusion Ignition Research Experiment (FIRE), An Option for a Major Next Step in Magnetic Fusion Research", Dale Meade, July (1999), http://fire.pppl.gov/Interim_Phys_Summ.doc.
3. M. Riccitelli, G. Vecchi, R. Maggiora, C. K. Phillips, R. P. Majeski, J. R. Wilson, D. N. Smithe, Fus. Eng. Design **45**, 1 (1999).
4. R. Majeski, "A Few RF Heating Scenarios for IGNITOR," presented at the IGNITOR Working Group Meeting, MIT, November 3-4, 1998.
5. code obtained from J. Jacquinot, private communication (1993).
6. E. F. Jaeger, D. B. Batchelor, and H. Weitzner, Nucl. Fusion **28**, 53 (1988).
7. "FIRE Ion Cyclotron System Design," D.W. Swain and M. D. Carter, Feb. 19, 1999 (unpublished memo).
8. M. D. Carter, D. A. Rasmussen, P. M. Ryan, et al., Nuclear Fusion **36**, 209 (1996).
9. J. R. Myra, D. A. D'Ippolito, and M. J. Gerver, Nucl. Fusion **30**, 845 (1990).
10. D. A. D'Ippolito, J. R. Myra, M. Bures and J. Jacquinot, Plasma Phys. and Controlled Fusion **33**, 607 (1991).
11. D. A. D'Ippolito and J. R. Myra, Phys. Plasmas **3**, 420 (1996).

RF Heating Studies for IGNITOR

J. R. Myra, D. A. D'Ippolito and R. E. Aamodt

Lodestar Research Corporation
Boulder, Colorado

M. D. Carter

Oak Ridge National Laboratory
Oak Ridge, Tennessee

Abstract

Two aspects of ICRF heating on IGNITOR are discussed in this report. The first topic is the use of high-frequency direct electron heating to provide an effective means of transitioning to the H-mode during the early ramped phase of the IGNITOR discharge when the magnetic field, plasma current and density are all increasing with time. It is shown that direct electron heating during the ramp phase is feasible at 400 MHz for IGNITOR parameters and can be used to reduce the required H-mode threshold power. The second topic considered here is an important problem in ICRF-edge physics, viz. the dissipation of power by rf sheaths on the antenna. It is shown that both the requirements of good heating efficiency and acceptable heat load on the antenna structure limit the allowed density at the antenna. This constraint must be taken into account in designing the IGNITOR antenna.

Table of Contents

I. Direct electron heating during the ramp-up phase

Introduction

A novel challenge presented by IGNITOR is that of rf heating during the B-field ramp. As explained subsequently, this is of interest for achieving an H-mode transition at low power, and in order to save transformer volt-seconds which must be conserved because of the relatively short pulse length. During the ramp the difficulty, not faced in conventional present day tokamak rf heating scenarios, is that the ion cyclotron resonance locations are moving for a fixed rf frequency. To circumvent the difficulties associated with undesirable edge resonances (especially near the antenna) and/or with engineering an rf system that uses variable or multiple frequencies, a direct electron heating scheme has been proposed utilizing high or medium harmonic fast waves.[1] Our work on scenario analysis for this scheme addresses the question of how direct electron rf heating can best be integrated with the B-field ramp. We wish to optimize absorption (an issue because of the less dense cooler plasma at the start of the ramp) to assist in obtaining an H-mode transition during the ramp (where the power threshold expected from empirical scalings should be lower than for flattop conditions).

In order to investigate tokamak operating conditions during the ramp we have developed a new kind of POPCON diagram in which the "y-axis" representing increasing n_0 is also used to represent increasing B and I_p. The x-axis is temperature as for the usual POPCONs. This allows consideration of startup scenarios. In particular, on the same diagram, we can show P_{aux}, single-pass absorption, the H-mode threshold and the parameter $Q = P_{fusion}/(P_{aux}+P_{oh})$. As we shall see, the topology of the P_{aux} contours for the ramped POPCON diagrams is similar to the conventional case, but the shape of the H-mode power threshold curves is different. Because the threshold power increases with density and B-field, it may be advantageous to make the transition into H mode during startup where B, n_0, and T are low. However, at low n_0 and T, the direct electron rf absorption is also poor, since it fundamentally scales with β_e and $k_{||}v_e/\omega$. It is important to understand the trade-offs involved to determine if direct electron heating during the ramp can be used to access the H-mode in IGNITOR.

Ramped POPCONs for the IOC scaling law

We first consider, in Fig. 1, the ramp phase under the Improved Ohmic Confinement (IOC) scaling law (Ohmic scaling without density saturation).[2] Shown are contours of P_{aux} (0, 2, 4, 6 MW, black), Q (5, 10, ∞, gold), where $Q = P_{fusion}/(P_{aux}+P_{oh})$ and the Troyon limit (green). The ramp is defined by varying n_0, B, and I_p linearly between the limiting values: $n_0 = (0, 1.2\ 10^{21})\ m^{-3}$, B = (5, 13) T, I_p = (0, 11) MA. For simplicity, the y-axis of the figure only shows the density variation (See Fig. 3 for the

corresponding variations of B and I_p.) Other IGNITOR parameters used for these studies are given in Table. I. The area of the contour plot with black shading corresponds to steady state power balance with $P_{aux} < 0$, therefore an Ohmic plasma ($P_{aux} = 0$) will evolve with $dW/dt > 0$ in the black region, moving the operating point to the right in the diagram when the density is held fixed. The IOC law gives $\tau \sim nq \sim nB/I_p$ so that in the scaled POPCON shown below $\tau \sim B$ and varies by about a factor of two over the whole contour plot, ranging from 0.4 s to 1.0 s. To understand the P_{aux} contours at low n_0 (I_p), note that $P_{oh} \sim I_p^2/T^{3/2}$ is negligible and that $P_{aux} \sim nT/\tau \sim T\, I_p / B$. Basically, the confinement is very good at the bottom of the ramp where q is large, and the density is low, so a little power goes a long way.

The plasma ignites (by any sensible definition) near the top of the ramp. Because the IOC law is so favorable, P_{rf} would probably not be required at all in this case. If it is, only a small amount would do.

An alternative way of presenting the scaled POPCON diagrams is to plot contours of $\lambda = W^{-1}\, dW/dt$ for a given P_{aux}. An example of such a diagram is shown in Fig. 2 for the case of the IOC law with $P_{aux} = 0$, i.e. a pure Ohmic discharge. Contour values are $\lambda = \{-4, -2, -1.5, -1., -0.5, 0, 0\ .5, 1., 1.5, 2., 4\}\ s^{-1}$ with the $\lambda = 0$ contour double. The ramp is defined as above. The plasma is heated ($\lambda > 0$) in the red shaded region and cooled ($\lambda < 0$) in the blue shaded region. Again, one sees that ignition occurs somewhere around $n_0 = 10^{21}\ m^{-3}$ and T = 11 keV.

While Figs. 1 and 2 are not directly relevant to rf heating of the ramp, we have presented them first because they are simpler to understand than the rf cases involving H-mode transitions presented next.

Ramped POPCONs and direct electron heating for the ITER-89p scaling law

The IOC law is much more optimistic than ITER-89p L mode scaling for IGNITOR, which we now consider (even though its application to high field tokamaks is probably unduly pessimistic). In L-mode we find that Q remains less than 5 over the accessible parameter space. Consequently, interesting performance requires an H-mode transition or performance with an effective H factor greater than one (relative to ITER-89p). We find that H = 1.8 is sufficient to yield ignition for a peaked profile case. To analyze the possibilities for ramp-up scenarios with rf-assisted H-mode access, we overlay the rf single pass absorption curves and the P_{aux} contours for the ramped POPCON. Again we use a linear ramp over the range $n_0 = 0 - 1.2 \times 10^{21}\ m^{-3}$, B = 5 - 13 T and I_p = 0 - 11 MA. The rf single pass absorption (f_{sp}) was calculated from the FREMIR[3] code for 400 MHz rf with $k_\parallel = 0.4\ cm^{-1}$. We take into account the different confinement

properties and rf absorption of three different phases: Ohmic, rf-heated L-mode, and H-mode.

The result is presented in Fig. 3 where we overlay the scaled POPCON P_{aux} contours, single pass absorption, Q, H-mode threshold and Troyon β limit for the ITER-89p law with H = 1.8. While the scaling of the threshold power necessary to transition into H-mode is still under investigation, here we consider the implications for IGNITOR of recent empirical data for diverted tokamaks.[4]

It can be seen from Fig. 3 that the single pass absorption is excellent (> 75%) once T exceeds 10 keV and one is at least 1/3 the way up the ramp ($n_0 > 4 \times 10^{20}$ m^{-3}, B > 8 T and I > 4 MA). However, single pass absorption appears to be an issue during the early startup phase where the plasma is cold, and or the density is very low. If one believes that H = 1.8 can only be achieved by obtaining an H-mode transition, then the P_{aux} contours of the diagram are self-consistent to right of the blue dashed line. This requires about 20 MW of absorbed rf power, after which ignition is readily achieved.

To analyze the start-up phase and rf-assisted H-mode transition in more detail, we must further complicate Fig. 3 by including a bifurcation in the confinement law using H = 1.0 below threshold and H = 1.8 above it. Results for the λ contours {-4, -2, -1.5, -1., -0.5, 0, .5, 1., 1.5, 2., 4}s^{-1} are presented in Fig. 4 for P_{aux} = 20 MW (absorbed into the core plasma). On the left of the diagram we have a region with H = 1.0 which terminates at the H-mode power threshold (heavy dashed line). On the right we have a region with H = 1.8 which begins at the H-mode power threshold. Here we assume the H-mode transition occurs when the conduction power equals the H-mode threshold power. The thick black lines are steady state (λ = 0) and the plasma is heated (λ > 0) in the red shaded region and cooled (λ < 0) in the blue shaded region. The diagram shows that there is a scenario to get to ignition, but it requires that the H-mode transition occur about half way or earlier up the ramp (where the plasma remains below 6×10^{20} m^{-3}). This follows from the figure because further up the ramp, the plasma is cooled λ < 0 at the H-mode transition boundary and therefore evolves away from the boundary to the left, back towards the heavy black λ = 0 contour. To make the transition at these higher values of n_0 and B would require P_{aux} > 20 MW. Assuming the operating point is moved to the transition boundary in the red region, the H-mode transition occurs. Once the transition is made, the burning and ignited plasma regimes are accessible. The gold contours shown in the figure are Q = {5, 10, 20}.

The blue rf absorption contours of Fig. 3 do not depend on the confinement properties of the plasma (i.e. the H value), and may be mentally overlaid on Fig. 4. The Ohmic target plasma at the bottom of the ramp is low density and cold, and is therefore a

poor absorber: we find that absorption becomes significant (f_{sp} > 25%) about half way up the ramp. Now applying rf, as the plasma heats, absorption improves to f_{sp} ~ 50% for 20 MW absorbed power at $n_0 = 6 \times 10^{20}$ m^{-3}, implying T_0 = 7 keV. This puts the plasma at the H-mode threshold. Once the transition to H-mode occurs, T_0 increase to about 12 keV, rf absorption is excellent, and there is a clear path to ignition for H ~ 1.8.

Choice of $k_{\|}$ for direct electron heating

The base case results discussed above were for the choice $k_{\|}$ = 0.4 cm^{-1}. In the following we discuss the effect of varying $k_{\|}$. In Fig. 5 below, the 10%, 25%, 50% and 75% contours of single pass absorption are shown in the scaled POPCON plane for the base case $k_{\|}$ = 0.4 cm^{-1} (blue) and for the case $k_{\|}$ = 0.2 cm^{-1} (gold).

Except at very low n_0, B, I_p (small values along the y-axis of the scaled POPCON diagram) absorption is an increasing function of $k_{\|}$ in the range $k_{\|}$ = 0.2 to 0.4 cm^{-1}. This can also be seen from Fig. 6 which shows the absorption vs. $k_{\|}$ for a fixed value along the y-axis of y = 0.45 (i.e. 45% up the ramp where $n_0 = 5.4\ 10^{14}$ cm^{-3}, B = 8.6 T) and for a fixed T_e = 6 keV. Significantly, at still higher values of $k_{\|}$ the accessibility of the rf wave becomes an issue due to the FW cutoff, as discussed next.

FW cutoff and lower hybrid resonance

When the density at the edge is low and $k_{\|}$ is large, the existence of the FW cutoff becomes important. This occurs at the start of the ramp, and is particularly an issue when the density profile is highly peaked, so that the edge to central density ratio is small. In the preceding discussion, it was shown that increasing $k_{\|}$ generally leads to improved absorption in the parameter range of interest. But this improvement comes at the cost of a greater difficulty in coupling to the wave, because the fields launched at the antenna must tunnel through the evanescent layer that occurs between the plasma surface and the FW cutoff.

To study the optimization of $k_{\|}$ would require a coupling code, capable of modeling the (waveguide) launcher. While this is beyond the scope of the present study, an idea of the acceptable range of $k_{\|}$ can be deduced from Fig. 7. In the vacuum, the evanescent scale length (for $k_y = 0$) is $k_{\|}^{-1}$; thus for acceptable coupling we expect that $k_{\|}$ $\Delta < g$ must pertain, where Δ is the layer width and g is a number of order unity, perhaps 2 or 3 at most. Thus, from Fig. 7 we expect that the useful range of $k_{\|}$ will be restricted to less than 0.5 cm^{-1}.

Effect of ramping xcenarios for B and n_0

The relatatively poor absorption at the bottom of the ramp in the preceding studies is due to the low β of the startup plasma. Direct electron absorption at fixed n_0 and T_e is, to an excellent approximation, linearly proportional to $1/B^2$ when the single pass absorption is small compared to one. (This has been checked numerically for the parameters of interest here, but is not illustrated.) Thus a possible method of further improving the absorption in the lower half of the ramp would be to consider scenarios where the density ramp begins at B values below 5 T. If this philosophy is to be pursued, other physics and engineering aspects of the ramp-up scenario would need to be re-examined, e.g. the Greenwald density limit and MHD stability limits.

Conclusions regarding direct electron heating during the ramp

Direct electron heating during the ramp appears to be feasible, based upon the results of this preliminary study. The main issue is the creation of an Ohmic target plasma which has sufficient single pass absorption to allow the heating to proceed, and hence the plasma to evolve to the higher T_e, where the direct electron absorption is better. A 400 MHz rf system is expected to perform best when the launched wavenumbers are in the approximate range $0.2\ cm^{-1} < k_{\|} < 0.5\ cm^{-1}$.

Under optimistic assumptions about the global energy confinement scaling (IOC scaling law) we find that IGNITOR ignites Ohmically, and the use of rf heating is not required. Under pessimistic assumptions (ITER-89p L mode scaling) interesting machine performance requires an H-mode transition. We find that the transition can be assisted by direct electron heating during the ramp. This strategy allows one to achieve H-mode access by making the transition at low density and B-field, where the threshold power for the transition is expected to be lower than for top-of-the-ramp parameters.

References for Part I

1. R. Majeski, presented at the US IGNITOR Working Group Meeting, MIT, Nov. 3-4, 1998.
2. J.A. Wesson, "Tokamaks" (Clarendon, Oxford, 1997), p. 176.
3. code provided by J. Jacquinot, private communication (1993).
4. K. Thomsen et al., ITER preprint, presented at the 17th IAEA Fusion Energy Conference, Yokohama, Japan, October 19 - 24, 1998.

Table I IGNITOR parameters employed in these studies.

R_0	1.32 m
a	0.47 m
δ	0.4
κ	1.87
B_0	13. T
I_p	11. MA
γ_n	2.
γ_T	2.
Z_{eff}	1.2
Z_{imp}	6.
f_{He}	0.

Figure Captions

1. Scaled POPCON (n_0, B, I_p vs. T) for the ramp phase of IGNITOR under the improved Ohmic Confinement (IOC) scaling law.
2. Scaled POPCON (n_0, B, I_p vs. T) for the ramp phase of IGNITOR under the improved Ohmic Confinement (IOC) scaling law, showing contours of the stored energy growth rate λ (s^{-1}).
3. Scaled POPCON (n_0, B, I_p vs. T) for the ramp phase of IGNITOR under the ITER-89p scaling law with H = 1.8.
4. Scaled POPCON (n_0, B, I_p vs. T) for the ramp phase of IGNITOR under the ITER-89p L mode scaling law (H = 1.0 left, and H = 1.8 right), showing contours of the stored energy growth rate.
5. Contours of single pass absorption at 10%, 25%, 50% and 75% in the scaled POPCON plane for the base case $k_{\|}$ = 0.4 cm^{-1} (blue) and for the case $k_{\|}$ = 0.2 cm^{-1} (gold).
6. Single pass absorption vs. $k_{\|}$ (cm^{-1}) for n_0 and B corresponding to 45% of the way up the ramp, for T_e = 6 keV.
7. Width of the FW cutoff layer Δ(cm) on the low field side of the tokamak vs. $k_{\|}$(cm^{-1}) for the same parameters as in Fig. 2.

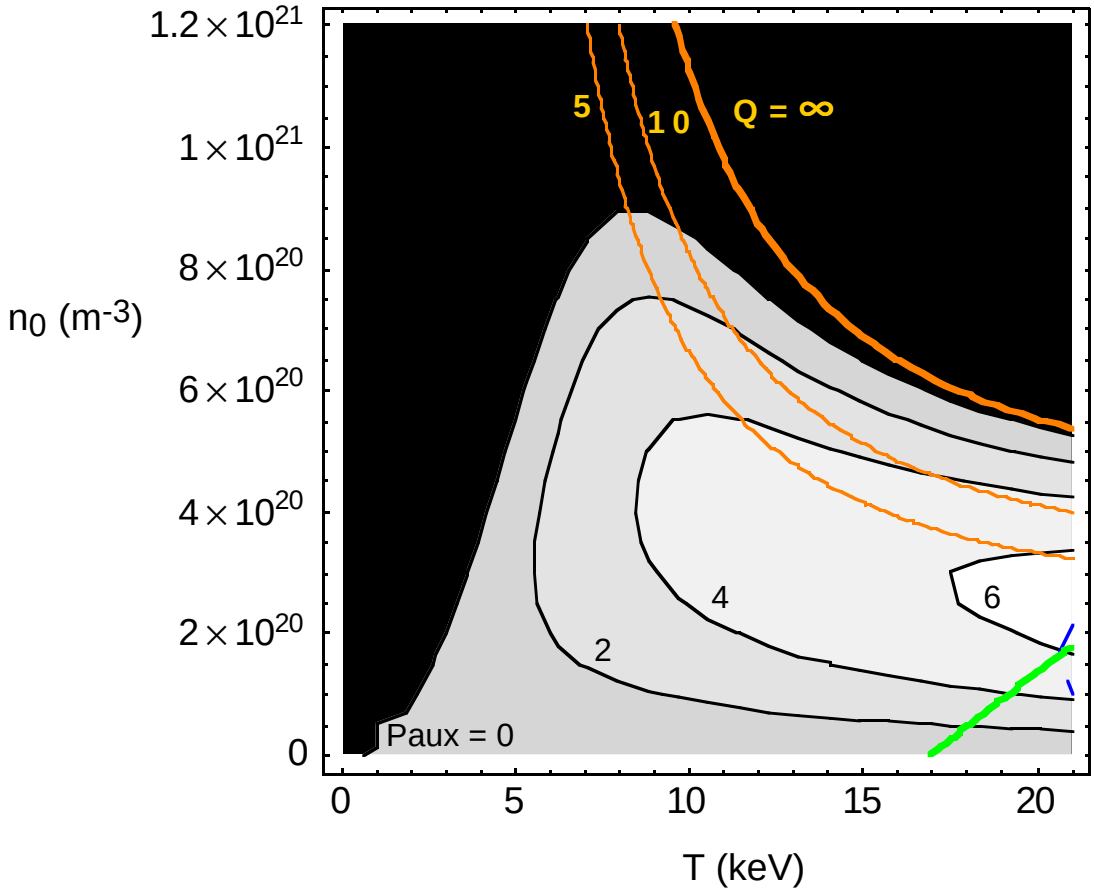
1.2×10^21
1×10^21
8×10^20
6×10^20
4×10^20
2×10^20
0
n0 (m-3)
0
5
10
15
20
T (keV)
5
10
Q = ∞
4
6
2
Paux = 0

Flg. 1

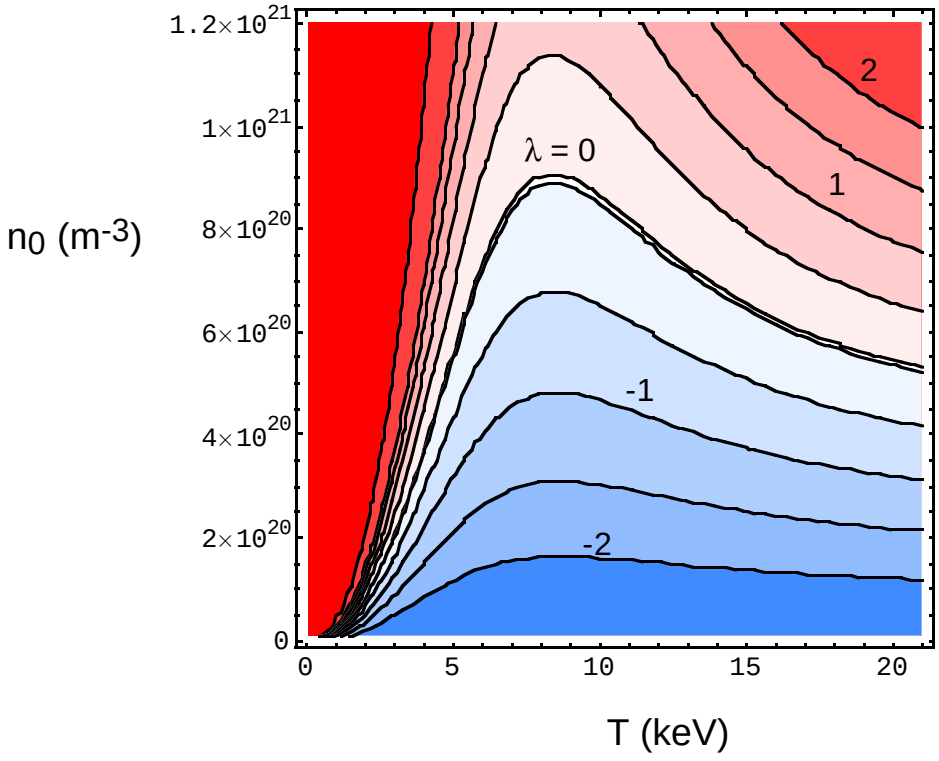
n_0 (m^{-3})
1.2×10^{21}
1×10^{21}
8×10^{20}
6×10^{20}
4×10^{20}
2×10^{20}
0
0
5
10
15
20
T (keV)
λ = 0
1
2
-1
-2

Flg. 2

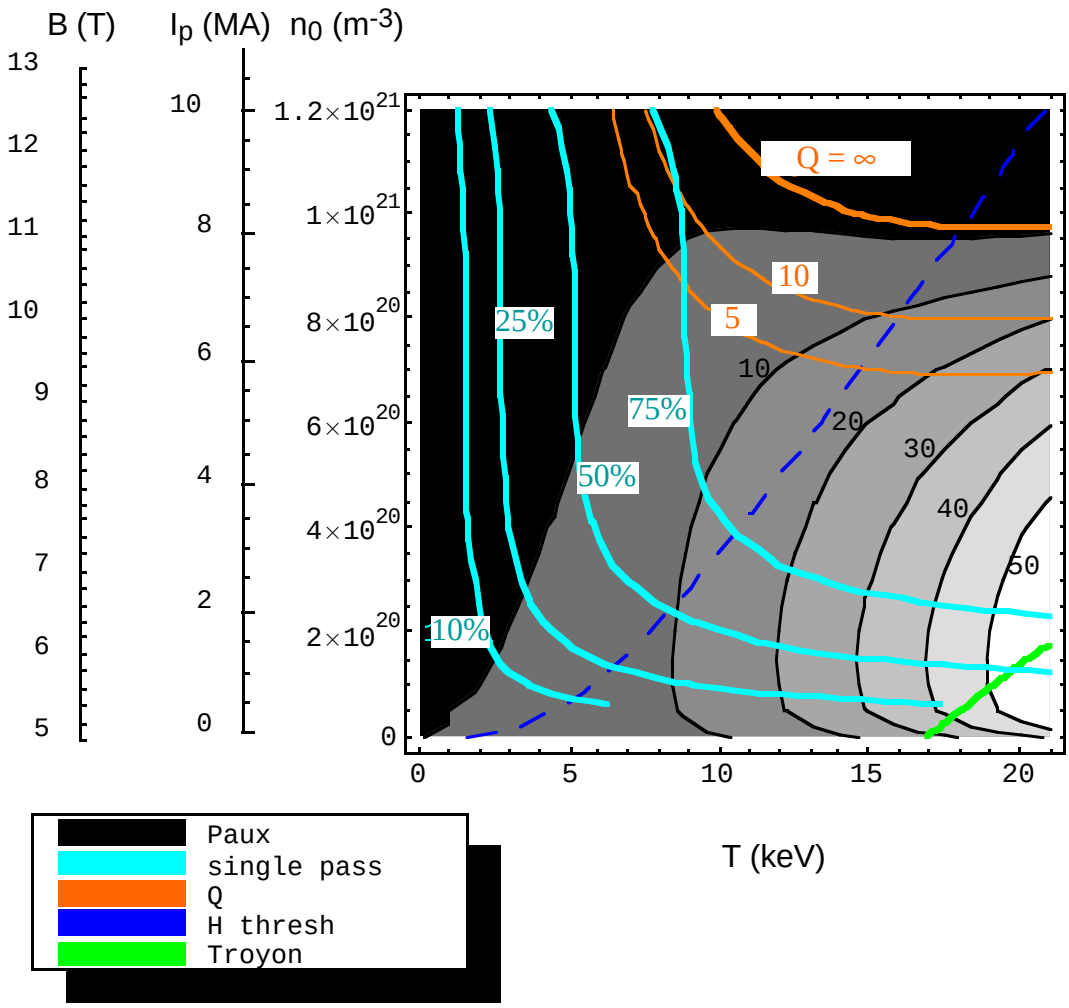
B (T)
I_p (MA)
n_0 (m^{-3})
13
12
11
10
9
8
7
6
5
10
8
6
4
2
0
1.2×10^{21}
1×10^{21}
8×10^{20}
6×10^{20}
4×10^{20}
2×10^{20}
0
Q = ∞
10
5
25%
10
75%
20
30
50%
40
50
10%
0
5
10
15
20
T (keV)
Paux
single pass
Q
H thresh
Troyon

Flg. 3

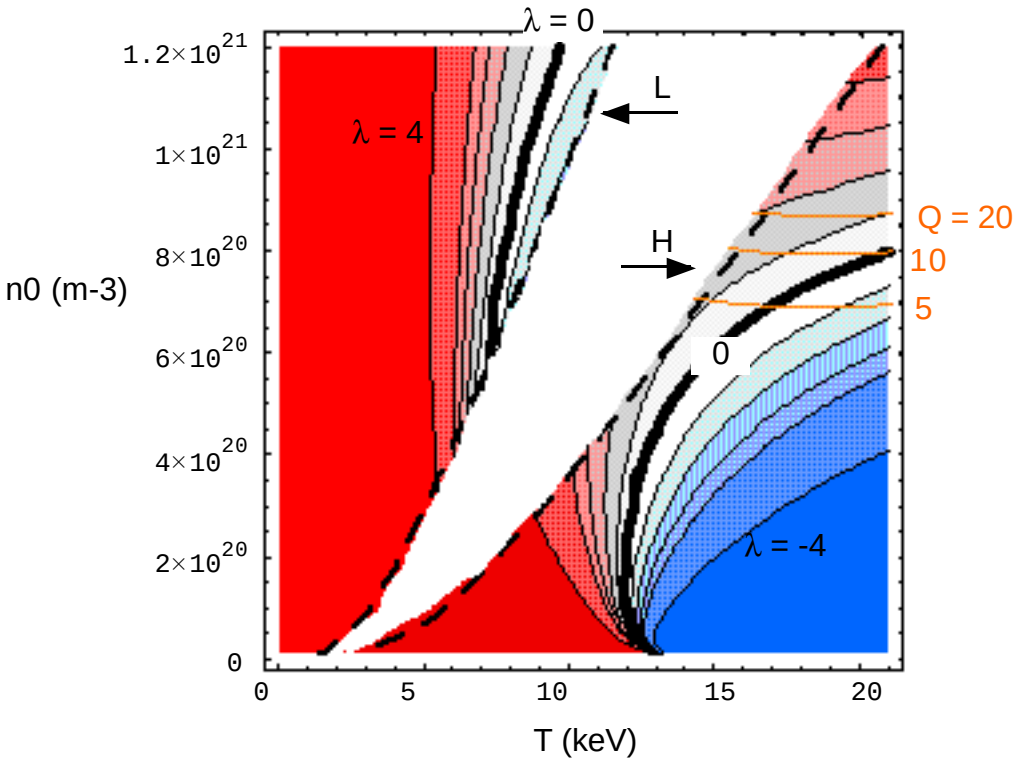
λ = 0
1.2×10^21
1×10^21
8×10^20
6×10^20
4×10^20
2×10^20
0
n0 (m-3)
λ = 4
L
H
Q = 20
10
5
0
λ = -4
0
5
10
15
20
T (keV)

FIg. 4

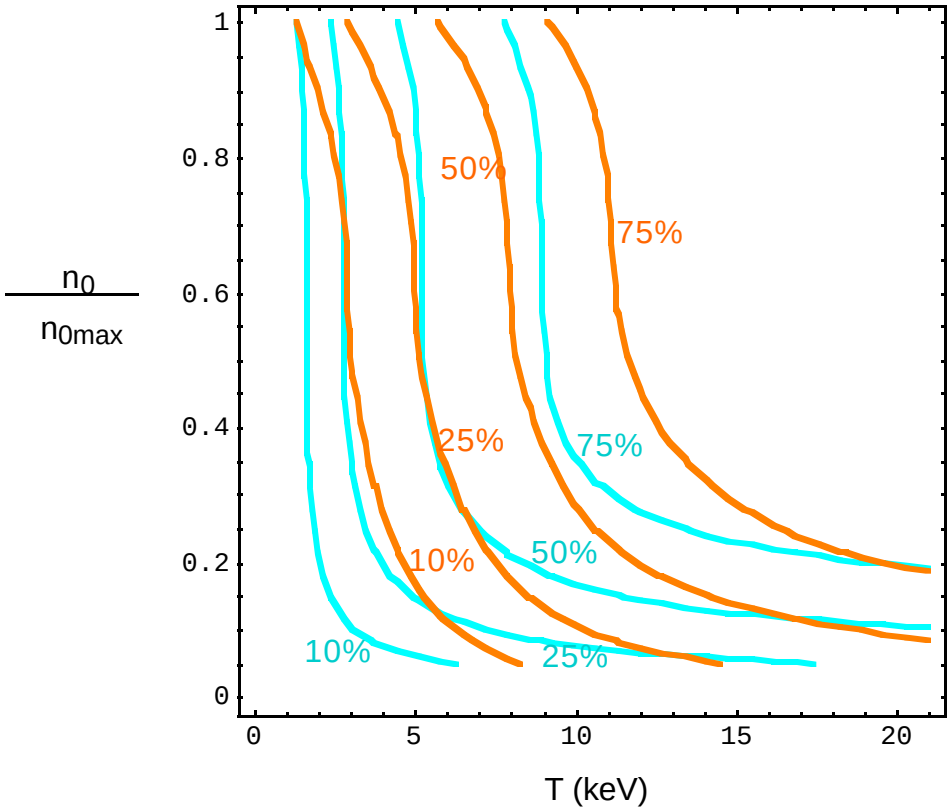

Flg. 5

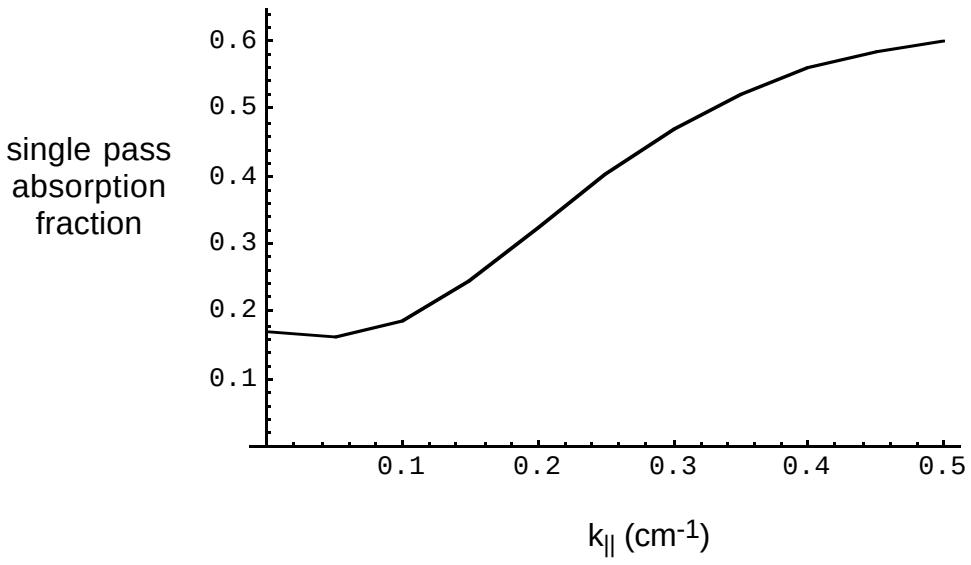
single pass
absorption
fraction
0.6
0.5
0.4
0.3
0.2
0.1
0.1
0.2
0.3
0.4
0.5
k|| (cm-1)

FIg. 6

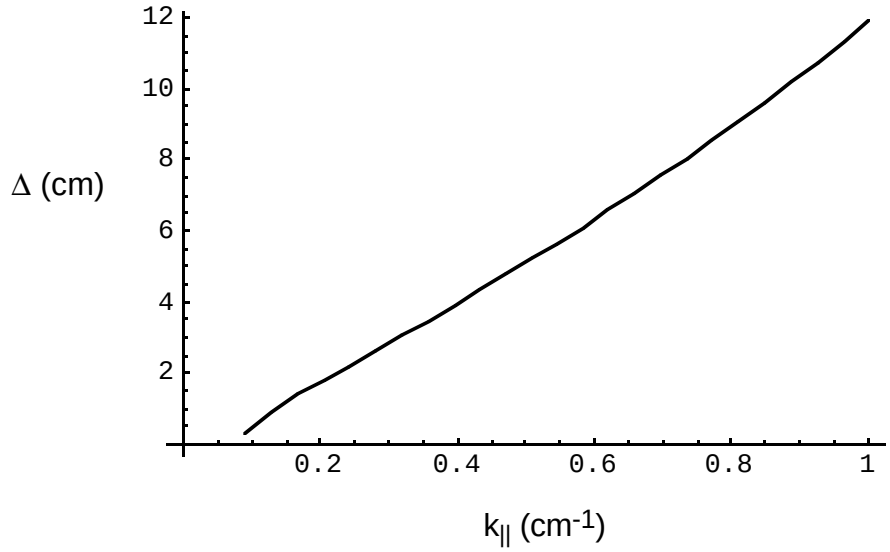
Δ (cm)
12
10
8
6
4
2
0.2
0.4
0.6
0.8
1
k|| (cm-1)

FIg. 7

II. ICRF edge interactions

Background

It is well-known that rf sheath formation on ICRF antennas produces a number of important and deleterious rf-edge plasma interactions that must be controlled for good antenna performance.[1-3] Recently a great deal of work has been carried out at Lodestar to understand rf sheath physics, develop theoretical models, and to benchmark these models against experimental data on JET, TFTR and DIII-D.[1-8] (References to work by other researchers can be found in these references.) Scaling studies[6] have shown that the most important sheath phenomenon for a high density machine like IGNITOR is power dissipation[5] by ions accelerated in the rf antenna sheaths. The power dissipated in the sheaths on the antenna and nearby limiter surfaces can reduce the overall heating efficiency of the antenna and cause an unacceptably large heat flux to these surfaces.

The present study evaluates these issues for the IGNITOR reference antenna design[9] (as of September, 1999) for ^{3}He minority heating during the flattop phase of the discharge. We obtain limits on the electron density to avoid reduced heating efficiency and limiter heat flux problems. It should be emphasized that these problems can always be eliminated by adequate protection of the antenna from the plasma using side limiters and a sufficiently large antenna-plasma separation. Optimization of the antenna and limiter design requires a low enough density at the antenna surface to reduce sheath effects to accepable levels, but a high enough density farther into the SOL to maintain good antenna coupling. The latter issue is not addressed in the present note.

Physics Model

We begin with a short summary of the relevant sheath physics, which depends on the following parameters: the local electron density n_e and temperature T_e at the antenna, the misalignment angle θ between the direction of the equilibrium magnetic field **B** and the bars of the Faraday screen (FS), the poloidal and toroidal dimensions of the full antenna (L_y and L_z), the number N of current straps in each antenna, the rf antenna voltage V_a along each current strap, the sheath driving voltage V_{rf}, and the rectified sheath voltage V_o at high density (full space charge). Here, all rf voltages will be specified as 0-to-peak values. The sheath driving voltage V_{rf} is defined as

$$V_{rf} = \int ds\, E_{\|}, \tag{1}$$

where $E_{||}$ is the component of the rf electric field parallel to **B**, induced by the mismatch of the equilibrium magnetic field with the antenna structure, and the integral is taken

along the magnetic field line between contact points with the antenna structure. In the usual limit $eV_{rf}/T_e >> 1$, simulations show that V_{rf} drives a rectified (DC) voltage $V_o \approx 0.6\ V_{rf}$,[1] where V_{rf} is the 0-peak value of the driving voltage. The resulting power dissipation P_{sh} by ions accelerated out of the plasma by the sheaths is given by[5] the product of the ion flux ($n_i\ c_s$), the energy gain (ZeV_o), and the total surface area A covered by the sheaths normal to **B** summed over both contact points ($A = 2\ A_n = 2\ L_x\ L_y$). It can be written in the form

$$P_{sh} = 1.9 \times 10^{-16}\ n_e\ (ZT_e/\mu)^{1/2}\ V_{rf}\ A_n\ , \qquad (2)$$

where the units of P_{sh}, A_n, n_i, T_e and V are kW, cm^2, cm^{-3}, eV and V, respectively. Note that the sheath power dissipation P_{sh} is linearly proportional to both the local density and the sheath voltage V_{rf}.

For idealized antennas with N straps, it is convenient to express V_{rf} on a given field line as follows:

$$V_{rf} = f\ N\ V_1 \equiv \frac{f\ L_z}{L_y} \tan\theta\ V_a\ , \qquad (3)$$

where V_1 is the sheath voltage drive per current strap and the other parameters were defined above. It is assumed in Eq. (3) that: (i) inductive (antenna current) coupling dominates capacitive (induced charge) coupling in determining the rf $E_{||}$ field; and (ii) the driving voltage difference V_{rf} occurs over the whole poloidal length L_y of the current strap. These assumptions are valid for the IGNITOR antenna. In Eq. (3), the figure-of-merit $f = V_{rf}/(N\ V_1)$ is the sheath voltage fraction for a given field line passing in front of the antenna, defined to lie in the range $0 < f < 1$. Physically, f is a measure of the degree of cancellation of the rf magnetic flux (or $E_{||}$) among the current straps. For an array of poloidally infinite current straps with adjacent straps out of phase (π phasing), the sheath voltage cancels ($f = 0$). An array with adjacent straps in phase (0 phasing) would have $V_{rf} = N\ V_1$ ($f = 1$). Even with π phasing, a real antenna (with finite length current straps and enclosed in a metallic box) will have a finite value of f because the rotational transform of the field lines breaks the antenna symmetry except for field lines at the antenna midplane and because of electrostatic charge effects near the corners of the antenna.

To characterize the IGNITOR antenna, the rf electric fields at the antenna are computed[10] using the RANT3D code[11] for the parameters $\theta = 9^\circ$, $L_y = 74$ cm, $L_z = 65$ cm, $N = 2$, and $P_{rf} = 4$ MW per antenna. The antenna is recessed in a rectangular cavity behind the first wall and the calculation of the electric fields includes the image currents in the metallic antenna box. The electric fields are scaled to give a coupled power of 4

MW per antenna. The antenna voltage V_a is computed by integrating E_y along the current strap from the voltage minimum to the voltage maximum, and one obtains V_a (peak-peak) = 70 kV at 4 MW. Although a FS is not explicitly modeled, an important aspect of the screen is retained by setting the electrostatic charges to zero ($\nabla \cdot \mathbf{J} = 0$) on the straps. The sheath calculation described here uses the rf electric field in the radial plane tangent to the first wall (referred to here as the "antenna surface"), which is the first surface on which the rf electric fields encounter significant plasma density. The sheath driving voltage is computed for each field line by carrying out the integral in Eq. (1) using the same magnetic field mapping as in the RANT3D run ($\theta = 9^\circ$). The antenna voltage V_a is calculated by integrating E_y along a current strap. Then Eq. (3) is inverted to obtain the distribution of f on the field lines passing in front of the antenna; this distribution is parameterized as $f(y_0)$, where y_0 is the poloidal coordinate of the field line at the toroidal center (z = 0) of the antenna. Finally the sheath power dissipation P_{sh} and the heat load $Q_{sh} = P_{sh}/A$ on the side limiters are calculated using Eq. (2) for an assumed density n_e at the antenna surface, where $A = 2\ A_n = 2\ L_x\ L_y$ is the total limiter area covered by the sheaths and where we let L_x be the radial decay length of the sheath potential at the antenna surface ($L_x \approx 0.5$ cm).

Two other ICRF-edge physics issues, viz. antenna impurity production and antenna arcing, will not be addressed here. Previous estimates[6] have shown that high-Z impurities from the antenna are heavily screened by ionization in the SOL plasma at the high densities typical of reactor machines; therefore, enhanced core radiation and dilution from these impurities is not a serious concern. Antenna arcing may well be an important problem, but a good model for antenna arcing is not available.

Results

The function $f(y_0)$ characterizing the sheath voltage distribution on the antenna is shown in Fig. 1 for the 2-strap IGNITOR antenna with π phasing between the straps. The maximum value f_{max} and average value <f> of this function are useful benchmarks of the sheath voltage distribution: we compute that $f_{max} = 0.35$ and <f> = 0.2. The corresponding values of sheath voltage are $V_{rf,max} = 3.5$ kV and $\langle V_{rf} \rangle = 2.2$ kV. The sheath voltage distribution along the antenna correlates with the field line position relative to the antenna geometry, as shown in Fig. 2. Here the color of each field line denotes its value of f or V_{rf}, as the two are proportional by Eq. (3), and hence its relative sheath voltage; the color scheme is chosen such that red indicates a large voltage and blue a small one. The field lines near the toroidal midplane ($y_0 = 0$) and field lines that miss

the antenna have low voltages; field lines that pass the two current straps asymmetrically and that pick up corner contributions have higher sheath voltages.

The presence of kV sheath voltages on field lines immersed in a relatively high edge density plasma is a concern, especially from the standpoint of sheath power dissipation. From Eqs. (2) and (3), the sheath power dissipation depends on the antenna properties (characterized by f), the magnetic field geometry (characterized by θ), and the local density n_e at the antenna surface. In Fig. 3, contours of P_{sh} in MW are plotted in the ($n_e - f\ \theta$) plane. This figure shows that choosing the antenna phasing to minimize f, aligning the magnetic field with the FS to minimize θ, and designing the antenna protection limiters to reduce n_e at the antenna surface all help to reduce P_{sh} to acceptable levels.

The main point illustrated by the sheath analysis is that even 2-strap antennas using π phasing can have large sheath potentials, and in high density tokamaks the sheath power dissipation can impose some design and operational constraints, viz. the antenna must be kept far enough from the plasma. To quantify this point, we have estimated the critical values of n_e at the antenna surface to maintain good heating efficiency and avoid overheating of the limiters. As a criterion for *good heating efficiency*, we require $P_{sh}/P_{rf} < 1/8$, where $P_{rf} = 4$ MW is the coupled power per antenna; we find that $P_{sh} < 0.5$ MW requires $n_e < 6 \times 10^{13}$ cm^{-3}, which is not hard to satisfy with the present IGNITOR design. Taking as the *heat load limit* on the antenna limiters the requirement that the peak heat load $Q_{sh} < 1$ kW/cm^2 implies the more stringent density requirement $n_e < 2 \times 10^{12}$ cm^{-3}. The IGNITOR antenna coupling and design studies should be carried out with these limitations in mind.

Although we have analyzed ICRF-edge interactions for conventional antennas in this section, our work motivates investigations of non-conventional ICRF launching techniques such as dielectric-filled and folded waveguides, possibly launching through a window. The latter would simplify hardware structures in the ignition plasma environment. The issues of obtaining sufficient $k_{||}$ for direct electron heating during the ramp as discussed in Sec. I (e.g. appropriate toroidal launch angles), and the role of SOL physics in the presence of intense fields near a wall, window or waveguide in these launching scenarios is an important area for future research.

References for Part II

1. J. R. Myra, D. A. D'Ippolito, and M. J. Gerver, Nucl. Fusion **30**, 845 (1990).
2. D. A. D'Ippolito, J. R. Myra, M. Bures and J. Jacquinot, Plasma Phys. and Controlled Fusion **33**, 607 (1991).
3. M. Bures et al. (JET), D. A. D'Ippolito and J. R. Myra, Plasma Phys. and Controlled Fusion **33**, 937 (1991).
4. D. A. D'Ippolito, J. R. Myra, J. Jacquinot, and M. Bures, Phys. Fluids B **5**, 3603 (1993).
5. D. A. D'Ippolito and J. R. Myra, Phys. Plasmas **3**, 420 (1996).
6. D. A. D'Ippolito and J. R. Myra, "Physical Scalings of ICRF-Edge Plasma Interactions," Bull. Am. Phys. Soc. **41**, 1427 (1996).
7. J. R. Myra, D. A. D'Ippolito and Y. L. Ho, Fusion Engineering and Design **31**, 291 (1996).
8. D. A. D'Ippolito, J. R. Myra, J. H. Rogers et al. (TFTR), G. R. Hanson et al. (ORNL), Nucl. Fusion **38**, 1543 (1998).
9. R. Maggiora, G. Vecchi, M. D. Carter, M. Riccitelli, Fus. Eng. Design **38**, 353 (1998).
10. M. D. Carter, D. B. Batchelor, D. W. Swain, S. L. Milora, R. Maggiora, G. Vecchi, "ICRF Modeling for IGNITOR," presented at the US IGNITOR Working Group Meeting, MIT, Nov. 3-4, 1998.
11. M. D. Carter, D. A. Rasmussen, P. M. Ryan, et al., Nuclear Fusion **36**, 209 (1996).

Figure Captions

1. Sheath voltage fraction f vs poloidal distance y_0 along the IGNITOR antenna.
2. Field lines labeled by sheath voltage fraction f (red $\rightarrow$ high voltage, blue $\rightarrow$ low voltage).
3. Contours of total sheath power dissipation at the antenna vs local density and antenna parameters (f = sheath voltage fraction, θ = B field misalignment angle)

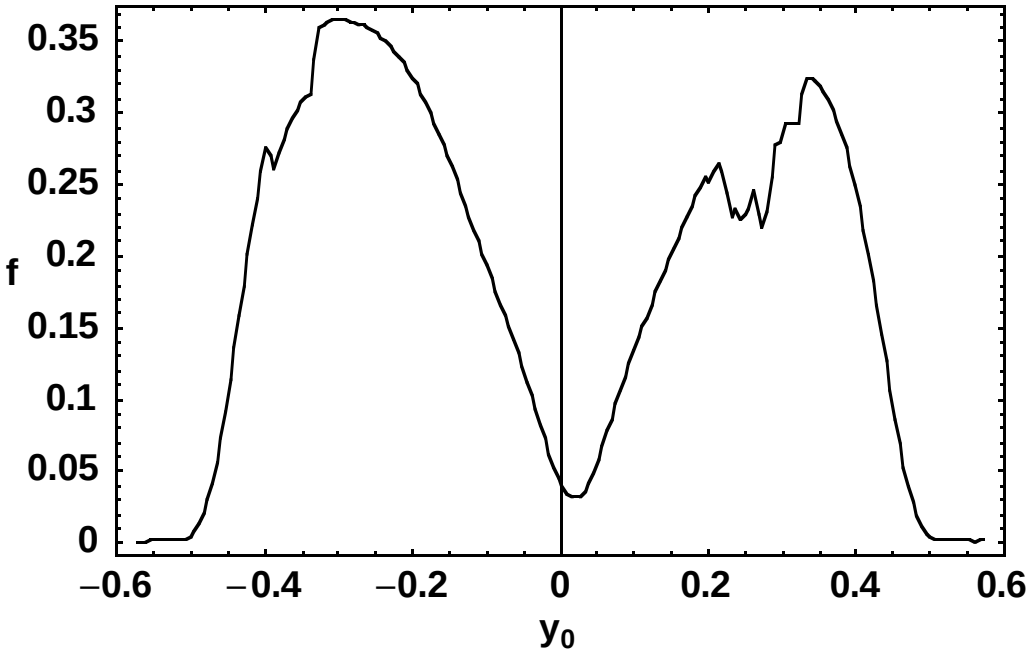

Fig. 1

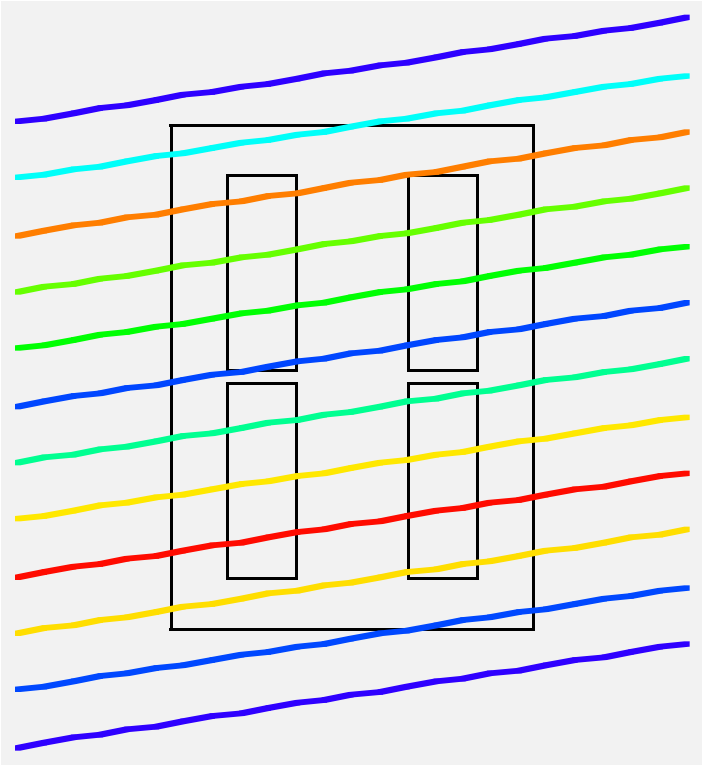

Fig. 2

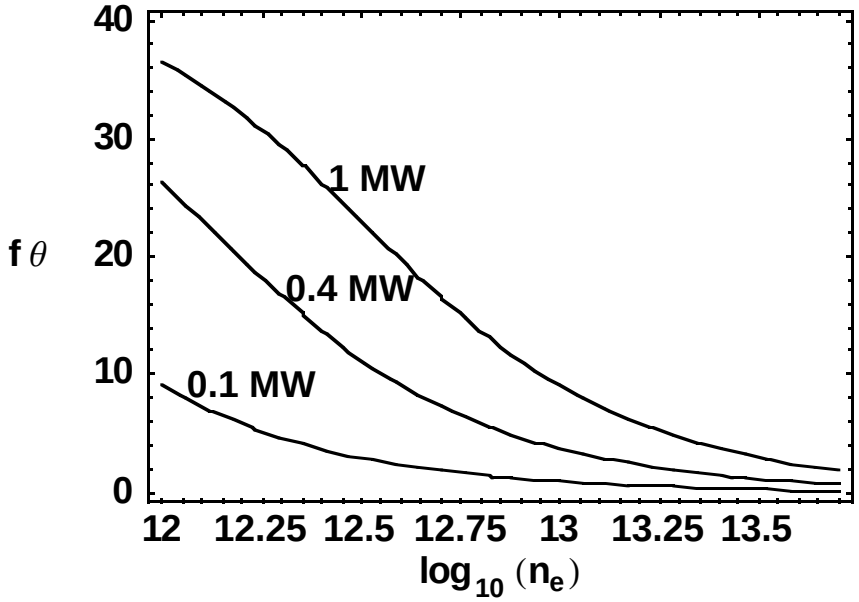
40
30
20
10
0
f θ
1 MW
0.4 MW
0.1 MW
12
12.25
12.5
12.75
13
13.25
13.5
log10 (ne)

Fig. 3

Acknowledgements

We wish to thank Dick Majeski for discussions of the high-frequency electron heating scenario for IGNITOR. This work was supported by the Raytheon/Lodestar subcontract No. 53250.420 7001; however, this support does not constitute an endorsement by either Raytheon or DOE of the views expressed herein.

RF Heating Studies for FIRE

D. A. D'Ippolito and J. R. Myra

Lodestar Research Corporation
Boulder, Colorado

M. D. Carter and E. F. Jaeger

Oak Ridge National Laboratory
Oak Ridge, Tennessee

Abstract

Two aspects of ICRF heating on FIRE are discussed in this report. The first topic is a survey of resonant second-harmonic ion and minority ion heating scenarios for the steady-state regime of the burning plasma. The single-pass absorption and fractional absorption by the various ion species is calculated as a function of minority ion and alpha concentration. It is shown that very good (> 90 %) single pass absorption can be obtained for any reasonable choice of parameters because of the high central density and large plasma size. For the optimal heating scenario, the single pass absorption is 100% and negligible power is coupled to the electrons and alpha particles, implying that ICRF is a very efficient means to heat the FIRE plasma. The second topic considered here is an important problem in ICRF-edge physics, viz. the dissipation of power by rf sheaths on the antenna. Implications of the present FIRE antenna design for rf sheath control are discussed, and it is shown that both the requirements of good heating efficiency and acceptable heat load on the antenna structure limit the allowed density at the antenna. This constraint must be taken into account in designing the FIRE antenna.

Table of Contents

I. Resonant ion heating of steady-state FIRE plasmas

Introduction

Ion cyclotron resonant heating (ICRF) is expected to play an important role in the FIRE burning plasma experiment. The present conceptual design calls for 30 MW of ICRF power in either a four or a six port system. The reference antenna design[1] calls for a single antenna in each port having two adjacent current straps with π relative phasing between the strap currents. Each strap has two coaxial feeds and is grounded at both ends. The antenna is electrically long at the frequencies of interest, with the phase of the current and voltage varying by about 2π radians along the strap. This "violin antenna" design has some unusual sheath properties which will be discussed in Sec. II. For the purposes of this section, it is sufficient to note that the launched $k_{\|}$ spectrum is nearly symmetrical about zero with peaks at $k_{\|} = \pm 9\ m^{-1}$.

The following machine parameters are assumed in Ref. 1 and in the present report: major radius R = 2 m, minor radius a = 0.5 m, and magnetic field on axis $B_0 = 10$ T. For this magnetic field, there are two reasonable scenarios for ion heating: (i) H minority or second harmonic D heating at 150 MHz, and (ii) He^3 minority or second harmonic T heating at 100 MHz. A survey of both heating scenarios are given in this report for the reference antenna design parameters using standard one-dimensional (1D) wave propagation codes. Questions of interest for each set of parameters include the single-pass absorption and the split of energy absorption among the various ion species (including alphas) and the electrons.

Two complementary 1D wave propagation codes have been used in this work. For convenience, most of the results presented here have been obtained with the FREMIR ray-tracing code developed by Jacquinot, which facilitates the computation of the single-pass absorption.[2] This code has been extensively benchmarked against the ORION1D full-wave code developed by Jaeger,[3] and good agreement is found between the codes. Typically, the single-pass absorption agrees to within 0.5 % and the dominant minority ion absorption to within 10-15%. A typical case is shown in Table 1. This case assumes an rf frequency of 100 MHz, $k_{||} = 9\ m^{-1}$, a 50:50 mixture of D:T, a 2% He^3 minority fraction with a tail temperature of 150 keV, a central electron density of $7\ 10^{14}\ cm^{-3}$, and a central $T_e = T_i = 10$ keV. Note that the agreement between the two codes is excellent and that the predicted single-pass absorption is greater than 95% with a small minority fraction.

Table 1 Comparison of wave absorption results computed from the FREMIR and ORION1D rf codes for a 50:50 mix of D:T with a 2% He^3 minority fraction.

	FREMIR	ORION1D
% single pass absorption	97.6	97.9
% electron absorption	11.3	8.4
% T absorption	9.5	12.6
% He^3 absorption	76.0	79.0

Survey of heating scenarios

In this section, we examine the single pass absorption and the distribution of energy among the particle species for both the He^3 and H minority ion heating scenarios. In all cases, we assume a 50:50 mixture of D:T and, for simplicity, a fixed minority tail temperature of 150 keV. The heating efficiency is computed as a function of minority ion and alpha particle concentration to tentatively identify the optimal heating scenario. These parameter scans are easily carried out using the 1D ray-tracing code FREMIR.

The analysis of the 100 MHz He^3 minority / second harmonic T heating scenario is shown in Fig. 1 as a function of the He^3 minority fraction. An alpha particle fraction of 0.5% was assumed for the ignited FIRE plasma. The single pass absorption is 91% for a He^3 concentration of 1% and increases to essentially 100% for 3.5% He^3. Most of the power is absorbed by the He^3 minority with a small fraction going to the T ions (via the second harmonic resonance) and to the electrons. Note that the power absorption by the D ions and alphas is negligible in this scenario because these ions are not resonant.

The analysis of the 150 MHz H minority / second harmonic D heating scenario is shown in Fig. 2 as a function of the H minority fraction., again assuming 0.5% of alpha particles. The single pass absorption is essentially 100% over the entire range shown. Again the minority ion species (here H) absorbs most of the power with only a small amount going to the electrons and other resonant ion species (alphas and second harmonic D).

The main qualitative difference between the two heating scenarios is that the power absorption by the alphas is negligible for He^3 minority heating but not negligible for H minority heating, because the alphas are resonant in the latter case. The dependence of the power split among species as a function of alpha concentration is shown in Fig. 3 for the minority H scenario. The fraction of power absorbed by the alphas reaches 34% for an alpha concentration of 1%. Similar results were obtained in an analysis of rf scenarios for IGNITOR.[4]

Conclusions

The main conclusion of this work is that both the 100 and 150 MHz scenarios proposed by Swain and Carter[1] are suitable for efficient heating in the FIRE experiment. Both have excellent single pass absorption and couple most of their power to the minority ion species at a centrally located resonance, allowing the possibility of peaked temperature profiles and good energy confinement. Electron heating by Landau damping and transit time pumping, which deposits the rf power over a broader fraction of the plasma cross-section, is less than 10% for a wide range of parameters. The main difference between the two scenarios is that alphas are resonant for the 150 MHz H-minority scenario. To the extent that the rf-heated alpha confinement is poorer than the minority plasma ions, it may be preferable to avoid the situation where 20-30% of the power is absorbed by the alphas. If the alpha fraction is greater than 0.5%, this consideration would favor the He^3 minority scenario. On the other hand, at a fixed electron density He^3 causes more dilution of the D/T fuel than does H. In either case, the present work shows that a range of high-efficiency ICRF scenarios exist for the FIRE experiment.

References for Part I

1. D. W. Swain and M. D. Carter, "FIRE Ion Cyclotron System Design," memo dated February 19. 1999.
2. code provided by J. Jacquinot, private communication (1993).
3. E. F. Jaeger, D. B. Batchelor, and H. Weitzner, Nucl. Fusion **28**, 53 (1988).
4. M. Riccitelli, G. Vecchi, R. Maggiora, C. K. Phillips, R. P. Majeski, J. R. Wilson, and D. N. Smithe, Fus. Engin. Design **45**, 1 (1999).

Figure Captions

1. Single pass absorption in FIRE as a function of the He^3 minority fraction for the 100 MHz heating scenario (He^3 minority and second harmonic T) .
2. Single pass absorption in FIRE as a function of the H minority fraction for the 150 MHz heating scenario (H minority and second harmonic D).
3. Single pass absorption in FIRE as a function of the alpha particle fraction for the 150 MHz heating scenario. Note that a significant fraction of power can be absorbed by the alphas in this case.

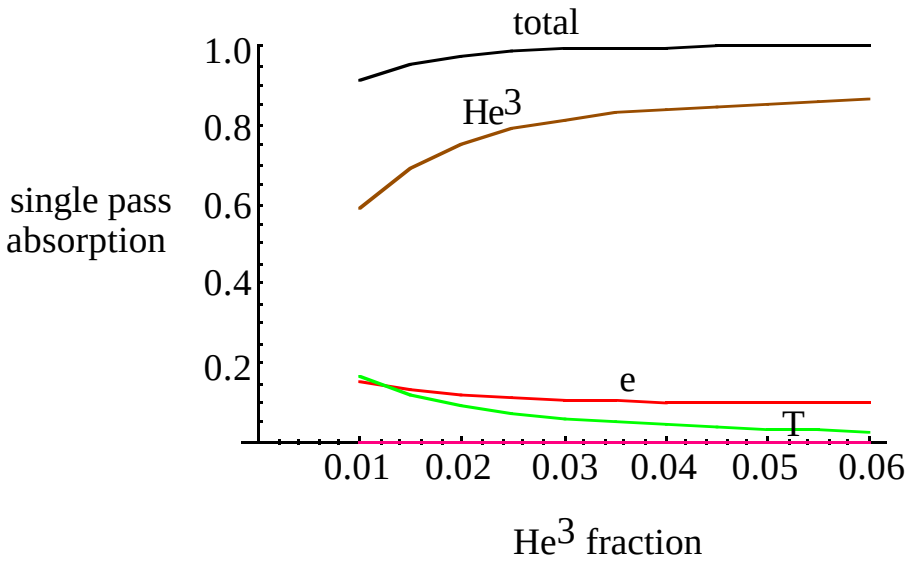
total
1.0
0.8
He3
single pass
absorption
0.6
0.4
0.2
e
T
0.01
0.02
0.03
0.04
0.05
0.06
He3 fraction

Fig. 1

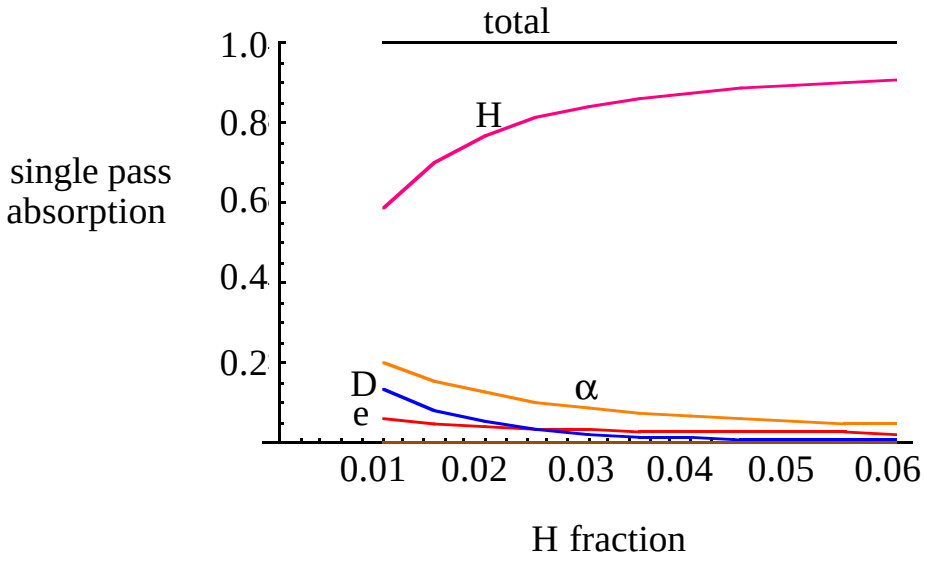
total
1.0
0.8
0.6
0.4
0.2
single pass
absorption
H
D
e
α
0.01
0.02
0.03
0.04
0.05
0.06
H fraction

Fig. 2

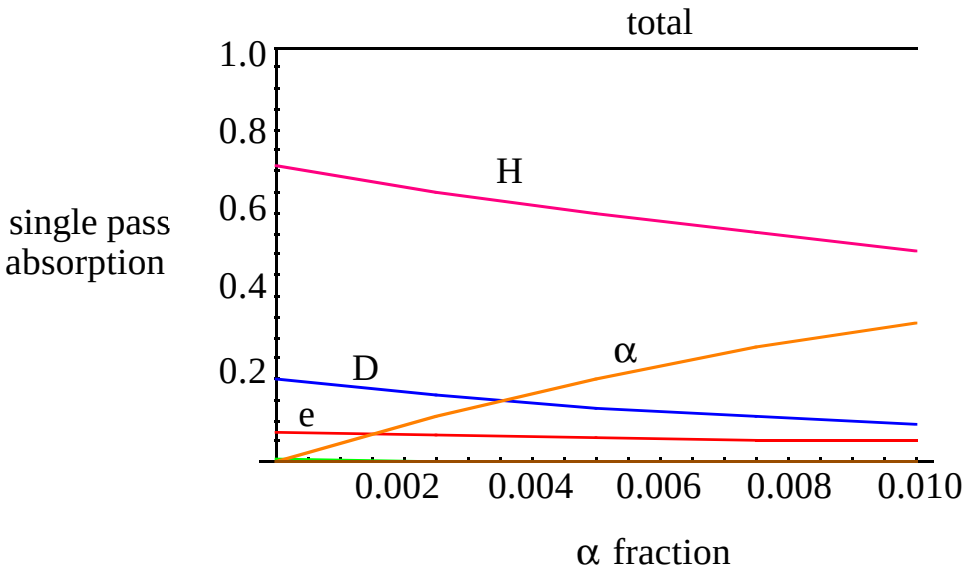
total
1.0
0.8
0.6
0.4
0.2
H
D
e
α
single pass
absorption
0.002
0.004
0.006
0.008
0.010
α fraction

Fig. 3

II. ICRF edge interactions

Background

It is well-known that rf sheath formation on ICRF antennas produces a number of important and deleterious rf-edge plasma interactions that must be controlled for good antenna performance.[1-3] Recently a great deal of work has been carried out at Lodestar to understand rf sheath physics, develop theoretical models, and to benchmark these models against experimental data on JET, TFTR and DIII-D.[1-8] (References to work by other researchers can be found in these references.) Scaling studies[6] have shown that the most important sheath phenomenon for a high density machine like IGNITOR is power dissipation[5] by ions accelerated in the rf antenna sheaths. The power dissipated in the sheaths on the antenna and nearby limiter surfaces can reduce the overall heating efficiency of the antenna and cause an unacceptably large heat flux to these surfaces.

The present study evaluates these issues for the FIRE reference antenna design as of September, 1999.[9] We obtain limits on the electron density to avoid reduced heating efficiency and limiter heat flux problems. It should be emphasized that these problems can always be eliminated by adequate protection of the antenna from the plasma using side limiters and a sufficiently large antenna-plasma separation. Optimization of the antenna and limiter design requires a low enough density at the antenna surface to reduce sheath effects to accepable levels, but a high enough density farther into the SOL to maintain good antenna coupling. The latter issue is not addressed in the present note.

Physics Model

We begin with a short summary of the relevant sheath physics. In the idealized model of an antenna which couples purely inductively, which we consider first for illustration, the sheath physics depends on the following parameters: the local electron density n_e and temperature T_e at the antenna, the misalignment angle θ between the direction of the equilibrium magnetic field **B** and the bars of the Faraday screen (FS), the poloidal and toroidal dimensions of the full antenna (L_y and L_z), the number N of current straps in each antenna, the rf antenna voltage V_a along each current strap, the sheath driving voltage V_{rf}, and the rectified sheath voltage V_o at high density (full space charge). Here, all rf voltages will be specified as 0-to-peak values. The sheath driving voltage V_{rf} is defined as

$$V_{rf} = \int ds\, E_{\|}, \tag{1}$$

where $E_{||}$ is the component of the rf electric field parallel to **B**, induced by the mismatch of the equilibrium magnetic field with the antenna structure, and the integral is taken along the magnetic field line between contact points with the antenna structure. In the usual limit $eV_{rf}/T_e >> 1$, simulations show that V_{rf} drives a rectified (DC) voltage $V_o \approx 0.6\ V_{rf}$, [1] where V_{rf} is the 0-peak value of the driving voltage. The resulting power dissipation P_{sh} by ions accelerated out of the plasma by the sheaths is given by[5] the product of the ion flux ($n_i\ c_s$), the energy gain (ZeV_o), and the total surface area A covered by the sheaths normal to **B** summed over both contact points ($A = 2\ A_n = 2\ L_x\ L_y$). It can be written in the form

$$P_{sh} = 1.9 \times 10^{-16}\ n_e\ (ZT_e/\mu)^{1/2}\ V_{rf}\ A_n\ , \qquad (2)$$

where the units of P_{sh}, A_n, n_i, T_e and V are kW, cm^2, cm^{-3}, eV and V, respectively. Note that the sheath power dissipation P_{sh} is linearly proportional to both the local density and the sheath voltage V_{rf}.

For idealized inductive antennas with N straps, it is convenient to express V_{rf} on a given field line as follows:

$$V_{rf} = f\ N\ V_1 \equiv \frac{f\ L_z}{L_y} \tan\theta\ V_a\ , \qquad (3)$$

where V_1 is the sheath voltage drive per current strap and the other parameters were defined above. In Eq. (3), the figure-of-merit $f = V_{rf}/(N\ V_1)$ is the sheath voltage fraction for a given field line passing in front of the antenna, defined to lie in the range $0 < f < 1$. Physically, f is a measure of the degree of cancellation of the rf magnetic flux (or $E_{||}$) among the current straps. For an array of poloidally infinite current straps with adjacent straps out of phase (π phasing), the sheath voltage cancels ($f = 0$). An array with adjacent straps in phase (0 phasing) would have $V_{rf} = N\ V_1$ ($f = 1$). Even with π phasing, a real antenna (with finite length current straps and enclosed in a metallic box) will have a finite value of f because the rotational transform of the field lines breaks the antenna symmetry except for field lines at the antenna midplane and because of electrostatic charge effects near the corners and sidewalls of the antenna. From Eq. (3) one can see that the sheath voltage depends on the antenna phasing (f), the magnetic field misalignment (θ), and the antenna voltage V_a (and thus indirectly on the rf power).

It is assumed in writing Eq. (3) and defining the quantity f that: (i) inductive (antenna current) coupling dominates capacitive (induced charge) coupling in determining the rf $E_{||}$ field; and (ii) the driving voltage difference V_{rf} occurs over the whole poloidal length L_y of the current strap. Our analysis of the RANT3D results (see below) shows that neither of these assumptions is satisfied by the present FIRE "violin"

antenna design. First, induced charge effects are important for this antenna; one finds that $E_{||}$ is dominated by the "capacitive" coupling contribution and does not show much cancellation along a given field line, so that the effective f in Eq. (3) is of order unity. Second, the electrical length of the antenna is about one wavelength, so that both the voltage and current vary by 2π radians along the current strap. Thus, the full 35 kV voltage variation occurs along the distance $L_y/4$, introducing an extra factor of 4 in the numerator of Eq. (3). Both of these effects tend to increase the antenna sheath voltages.

To quantify these effects for the FIRE antenna geometry, the rf electric fields at the antenna are computed[9,10] using the RANT3D antenna code[11] for the parameters $\theta = 11^\circ$, $L_y = 118.8$ cm, $L_z = 65.2$ cm, $N = 2$, and $P_{rf} = 5$ MW per antenna. The antenna is recessed in a rectangular cavity behind the first wall and the calculation of the electric fields includes the image currents in the metallic antenna box. The electric fields are scaled to give a coupled power of 5 MW per antenna, assuming that six ports are available for ICRF. The antenna voltage V_a is computed by integrating E_y along the current strap from the voltage ground to the voltage maximum, and one obtains V_a (peak-peak) = 35 kV at 5 MW. Although a FS is not explicitly modeled, an important aspect of the screen is retained by setting the electrostatic charges to zero ($\nabla \cdot \mathbf{J} = 0$) on the straps. The sheath calculation described here uses the rf electric field in the radial plane tangent to the first wall (referred to here as the "antenna surface"), which is the first surface on which the rf electric fields encounter significant plasma density. The maximum sheath driving voltage V_{rf} is computed for each field line by carrying out the integral in Eq. (1) using the same magnetic field mapping as in the RANT3D run ($\theta = 11^\circ$). The integral is carried out across the antenna box in front of both straps to give a worst case estimate, as there is no cancellation between straps due to capacitive (induced charge) effects. To get a lower bound on the sheath voltage, we note that there are two effects which may reduce the sheath voltage in the experiment below this estimate. First, the presence of a FS (not modeled here) will substantially reduce the $E_{||}$ field seen by the plasma. Estimates based on the decay of $E_{||}$ in the plasma region of the RANT3D simulation suggest that this effect will reduce the sheath voltage by a factor of 1/2. Second, the electron transit distance along the field line in one rf period is much shorter than the toroidal width of the antenna; consequently, the electrons in the vicinity of one current strap may not be affected by the $E_{||}$ field in front of the other current strap, reducing the driving voltage by another factor of 1/2. Thus, we will use $V_{rf}/4$ as an estimate of the lower bound and V_{rf} as an upper bound on the sheath voltage.

As one measure of the sheath effect, we compute the voltage distribution $V_{rf}(y_0)$ and the average $\langle V_{rf} \rangle$ of this distribution over y_0, where y_0 is the poloidal coordinate of

the field line at the toroidal center (z = 0) of the antenna. Finally the sheath power dissipation P_{sh} and the heat load $Q_{sh} = P_{sh}/A$ on the side limiters are calculated using Eq. (2) for an assumed density n_e at the antenna surface, where $A = 2\ A_n = 2\ L_x\ L_y$ is the total limiter area covered by the sheaths and where we let L_x be the radial decay length of the sheath potential at the antenna surface ($L_x \approx 0.5$ cm).

Two other ICRF-edge physics issues, viz. antenna impurity production and antenna arcing, will not be addressed here. Previous estimates[12] have shown that high-Z impurities from the antenna are heavily screened by ionization in the SOL plasma at the high densities typical of ignition machines; therefore, enhanced core radiation and dilution from these impurities is not a serious concern. Antenna arcing may well be an important problem, but a good model for antenna arcing is not available.

Results

The function $V_{rf}(y_0)$ characterizing the sheath voltage distribution on the antenna is shown in Fig. 1 for the 2-strap FIRE antenna with π phasing between the straps. The maximum value $V_{rf,max}$ and average value $<V_{rf}>$ of this function are useful benchmarks of the sheath voltage distribution: for this antenna we compute that $V_{rf,max} = 4.4$ kV and $<V_{rf}> = 2.8$ kV. The sheath voltage distribution along the antenna correlates with the field line position relative to the antenna geometry, as shown in Fig. 2. Here the color of each field line denotes its relative sheath voltage V_{rf}; the color scheme is chosen such that red indicates a large voltage and blue a small one. The field lines with the highest voltages pass in front of the two feeders for each current strap. From the RANT3D electric field solutions, it appears that a large capacitive voltage is induced between the current straps and the sidewalls of the antenna box at the poloidal location of the feeders. One a given field line, the sign of the $E_\parallel$ generated by these voltage differences is the same in the vicinity of each current strap, despite the π phasing of the currents in the straps. Thus, the capacitive effects associated with the feeders prevent the reduction of the sheath voltages in π phasing obtained for the case of purely inductive coupling. The lowest sheath voltages occur on the field lines near the toroidal midplane ($y_0 = 0$), which are half-way between the two feeders, and on field lines that miss the antenna. The presence of kV sheath voltages on field lines immersed in a relatively high edge density plasma is a concern, especially from the standpoint of sheath power dissipation.

The main point illustrated by the sheath analysis is that even 2-strap antennas using π phasing can have large sheath potentials, and in high density tokamaks the sheath power dissipation can impose some design and operational constraints, viz. the antenna must be kept far enough from the plasma. To quantify this point, we have estimated the

critical values of n_e at the antenna surface to maintain good heating efficiency and avoid overheating of the limiters. As a criterion for *good heating efficiency*, we require $P_{sh}/P_{rf} < 1/8$, where $P_{rf} = 5$ MW is the coupled power per antenna; we find that $P_{sh} < 0.6$ MW requires $n_e < 1 - 5 \times 10^{13}$ cm^{-3}, where the lower (upper) density estimate corresponds to the upper (lower) bound on V_{rf}. Taking as the *heat load limit* on the antenna limiters the requirement that the peak heat load $Q_{sh} < 1$ kW/cm^2 implies the more stringent density requirement $n_e < 0.2 - 1 \times 10^{13}$ cm^{-3}. The FIRE antenna coupling and design studies should be carried out with these limitations in mind.

References for Part II

1. J. R. Myra, D. A. D'Ippolito, and M. J. Gerver, Nucl. Fusion **30**, 845 (1990).
2. D. A. D'Ippolito, J. R. Myra, M. Bures and J. Jacquinot, Plasma Phys. and Controlled Fusion **33**, 607 (1991).
3. M. Bures et al. (JET), D. A. D'Ippolito and J. R. Myra, Plasma Phys. and Controlled Fusion **33**, 937 (1991).
4. D. A. D'Ippolito, J. R. Myra, J. Jacquinot, and M. Bures, Phys. Fluids B **5**, 3603 (1993).
5. D. A. D'Ippolito and J. R. Myra, Phys. Plasmas **3**, 420 (1996).
6. D. A. D'Ippolito and J. R. Myra, "Physical Scalings of ICRF-Edge Plasma Interactions," Bull. Am. Phys. Soc. **41**, 1427 (1996).
7. J. R. Myra, D. A. D'Ippolito and Y. L. Ho, Fusion Engineering and Design **31**, 291 (1996).
8. D. A. D'Ippolito, J. R. Myra, J. H. Rogers et al. (TFTR), G. R. Hanson et al. (ORNL), Nucl. Fusion **38**, 1543 (1998).
9. D. W. Swain and M. D. Carter, "FIRE Ion Cyclotron System Design," memo dated February 19. 1999.
10. M. D. Carter, private communication (1999).
11. M. D. Carter, D. A. Rasmussen, P. M. Ryan, et al., Nuclear Fusion **36**, 209 (1996).

Figure Captions

1. Sheath voltage V_{rf} in kV vs poloidal distance y_0 in meters along the FIRE antenna.
2. Field lines labeled by sheath voltage (red $\rightarrow$ high voltage, blue $\rightarrow$ low voltage).

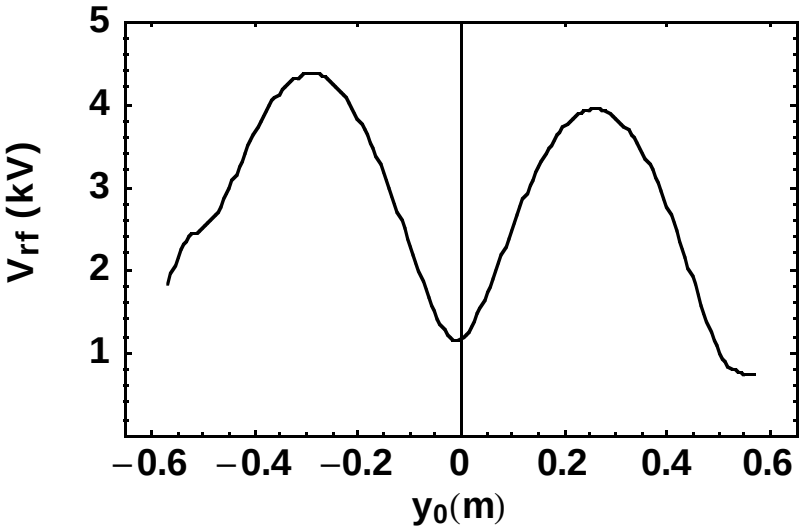

Fig. 1

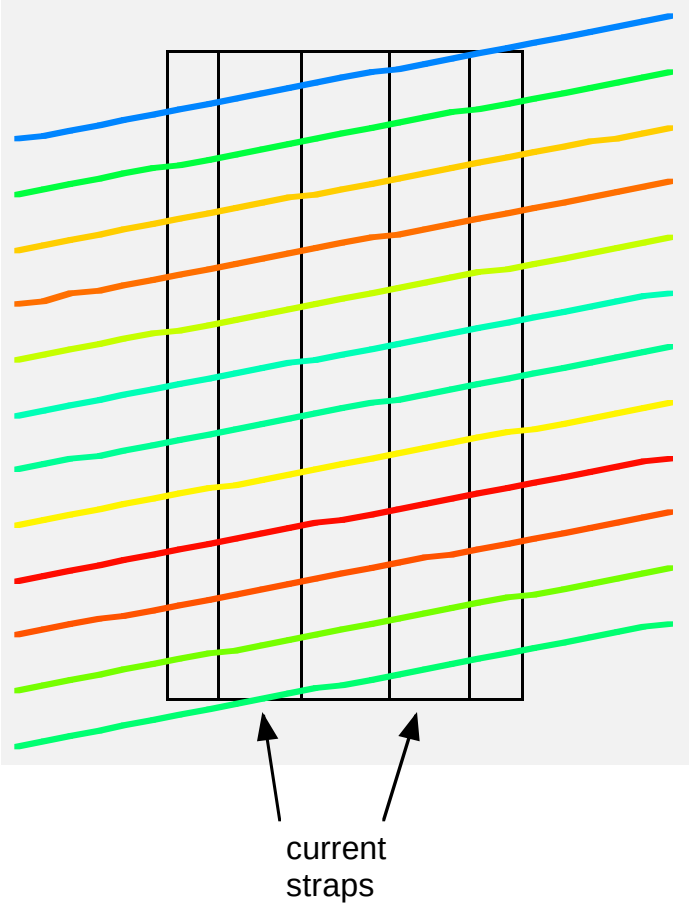

Fig. 2

Acknowledgements

This work was supported by the Raytheon/Lodestar subcontract No. 53250.420 7001; however, this support does not constitute an endorsement by either Raytheon or DOE of the views expressed herein.